Supporting Information

Cartault et al. 10.1073/pnas.1111596109

SI Methods

Knockdown of SLC7A2-IT1A/B with Antisense Oligonucleotides. Kelly neuroblastoma cells (Health Protection Agency culture collection N° 92110411) were cultured at 37 °C in a humidified atmosphere containing 5% CO_2 (vol/vol) in RPMI medium with 10% FCS (vol/vol), penicillin (100 mg/mL), streptomycin (100 U/mL), sodium pyruvate (1 mM), L-glutamine (5 mM), and Fungizone (0.5 mg/mL). Phosphorothioate-modified antisense oligonucleotide A-AAAGGAGGGAGAAGGAGGG (AS-A) and phosphorothioate-modified antisense oligonucleotide L1-ATACATGGGCAGAACACAC6 (AS-L1) (both from Integrated DNA Technologies) were used at 50 nM. The commercially available scrambled oligonucleotides from Ambion was used for mock. Cells were transfected using DharmaFECT1 (Dharmacon) following the manufacturer's protocol. Cells were harvested 12, 24, and 48 h posttransfection and total RNA was extracted and used for quantitative RT-PCR (qRT-PCR), as described in the main text. For analysis of cell-death markers, cells were grown and transfected on glass cover-slips. The cells were fixed in 3.7% paraformaldehyde (wt/vol) for 30 min, permeabilized by immersion in cold ethanol for 5 min, and conserved at –20 °C before incubation with the mouse anti-human Bax clone 2D2 (eBiosciences) and rabbit polyclonal anti-active Caspase-3 (BioVision) primary antibodies (1/200). After 1 h in PBS-BSA 1% at room temperature, cells were washed with PBS thrice and incubated with Alexa488- or Alexa594-conjugated anti-mouse or anti rabbit IgG (1/1,000) (Invitrogen, Molecular Probes). Nuclear morphology was revealed by addition of DAPI (final concentration: 100 ng/mL). Cells were mounted in Vectashield solution, and fluorescence was observed under a Nikon Eclipse E2000-U microscope, G 400×, and images taken using the NikonDigital sight PS-U1 camera system with NISElement AR imaging software. Results are expressed as percentage of cells stained for mitochondrial Bax (Bax^+) and active Caspase-3 (cleaved-caspase3^+). All results are expressed as mean percentage ± SD of three independent experiments, each in triplicate. The comparison between different treatments was analyzed by the Mann–Whitney exact test (Graphpad). *P* values below 0.05 were considered statistically significant.

Table of primers and oligonucleotides used in this study

O`ligonucleotide/primer name	Sequence 5′ to 3′	Sequence reference
IT1-A/B-F	GTAGTAACAAATTTGTCCGCA	ENST00000494857*
IT1-A/B-R	GGCAGAACACACAGGTTTGT	ENST00000494857*
IT1-A-F	ACCCGGAGTCCCCGTTGTGC	Fig. S4
IT1-A-R	TGTCCACCAAAGGGCACCAAAGT	Fig. S4
SLC7A2-E4-F	CTTCGTCAGACGTCAGAATG	ENST00000470360*
SLC7A2-E4-R	TGATGTACCTATCACATACGA	ENST00000470360*
VIME1-F	ACCAGCTAACCAACGACAAA	NM_003380†
VIME4-R	TGCTGTTCCTGAATCTGAGC	NM_003380†
GAPDH-E3-F	GAACGGGAAGCTTGTCATCA	ENST00000229239
GAPDH-E3-R	TGACCTTGCCCACAGCCTTG	ENST00000229239
MTMR7-E7-F	GCTGGAAGTGTGTGAACTTA	ENST00000180173
MTMR7-E7-R	CATCTAGATTGCCATATCGG	ENST00000180173
NAV1-E13-F	TTCTGCCAATGCTAATCTGG	ENST00000367296
NAV1-E13-R	ATCCGAAGTTCTTTGGGTGT	ENST00000367296
β-Actin-F	TGAAGTGTGACGTGGACATC	
β-Actin-R	GTCATAGTCCGCCTAGAAGC	
30‡ (Stealth RNAi)	AGCCCUUGUUUCUCCUGGCUGUUAU	Fig. S4
589‡ (Stealth RNAi)	GGUGCAUCAUUUGAAUGCUUUGUCA	Fig. S4
1325‡ (Stealth RNAi)	GGAAAUGUUGUGGAUGAUAUUGACA	Fig. S4
1496‡ (Stealth RNAi)	AAACCUGUGUGUUCUGCCCAUGUAU	Fig. S4
AS-A (phosphorothioate, IDT)	AAAGGAGGGAGAAGGAGGG	Fig. S4
AS-L1(phosphorothioate, IDT)	ATACATGGGCAGAACACAC	Fig. S4

*Ensembl accession number.
†GenBank accession number.
‡Nucleotide position correspond to those in the transcript A (Fig. S4).

Natural History and Clinical Features of the Disease. Reunion is a French island located in the Indian Ocean, at about 400 miles east of Madagascar and 100 miles south west of Mauritius. Reunion Island is roughly elliptical, 40 miles in length and 30 miles in width. One still active volcano has been redesigning the landscape and peopling of the island for several decades. Originally uninhabited, this region was colonized by the French in 1665. The East India Company contributed to the settlement of various populations of Europe, Africa, Madagascar, and India. The population increased quickly with immediate admixture. From 1715, Reunion Island experienced an economic burst based on the production of coffee and spices, subsequently replaced by sugar cane (1). This latter production was remarkably labor intensive, and thus resulted in the introduction of slaves from the coasts of Africa and Madagascar. After slavery was abolished in 1848, "enlisted" workers were enrolled from the southeast coasts of the Indies. Other voluntary immigrants comprised Indians from Gujarat and Chinese from various regions, all of whom established communities. As a consequence, successive settlements by European, African, Malagasy, Indian, and Chinese

immigrants led to a concentration of ethnic mixing, as well as the formation of many isolates in which consanguinity was high. Thus, because of the combination of socioeconomic and geographic constraints, genetic diseases like congenital adrenal hyperplasia, Friedreich ataxia, and calpainopathy are particularly frequent in the Reunion Island.

Infantile anorexia with vomiting seemed to be more common in some discrete regions of Reunion. In 1999, we had originally reported 24 cases with RAVINE syndrome that consisted in anorexia, irrepressible vomiting, and neurological signs in patients originating from the Reunion Island (2). At that time, we could not rule out the association with other diseases and thus heterogeneity of this group remains plausible. Furthermore, clinical features overlapped the phenotypes of other leukoencephalopathies, including Leigh disease and vanishing white-matter disease (3). In the present study, inclusion criteria of patients, which are synthesized in Table S1, were based on anorectic behavior with irrepressible and repeated vomiting during infancy, which was related to acute brainstem dysfunction (laryngeal paralysis and motor ocular abnormalities) and led to severe failure to thrive together with a specific involvement of the posterior fossa upon MRI. After the age of 2 y, patients present relapse emesis and mild psychomotor delay with cerebellar and pyramidal tract involvement. After 10 y of age, stress or mild head shock with acute neurologic involvement leads to coma during the terminal course of the disease. MRI of patients reveals progressive and severe vanishing of the cerebellar white matter and brainstem atrophy, as well as sus-tentorial periventricular white matter hyperintensities associated with basal ganglia anomalies (Fig. 1*B*).

1. Combeau Y, Maestri E (2002) *History of the Reunion Island: Colonial to Regional History* (French) (Nathan, Paris), pp 1–159.
2. Renouil M, et al. (1999) Severe anorexia in infants in Reunion: A new autosomal recessive disease? (French) *Arch Pediatr* 6:725–734.
3. Leegwater PA, et al. (2001) Subunits of the translation initiation factor eIF2B are mutant in leukoencephalopathy with vanishing white matter. *Nat Genet* 29:383–388.

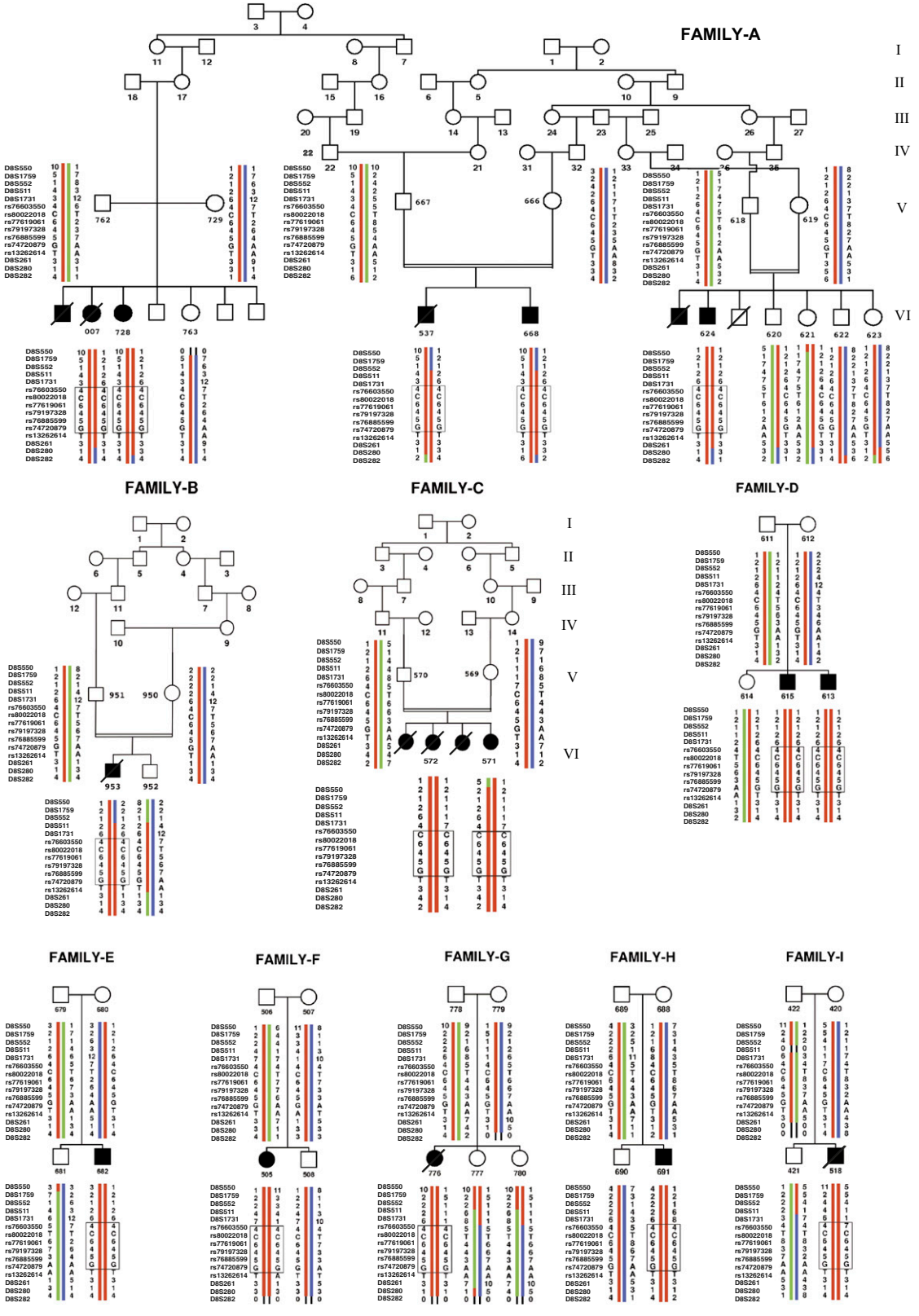

Fig. S1. Pedigrees of families and haplotype reconstruction in families for 8p markers. Families are named A to I. Affected and unaffected individuals are represented by black and open symbols, respectively. Additional slashes indicate deceased patients. Fine-mapped minimal regions are boxed.

A.

MARKER	LOD SCORES AT θ = 0.00	0.01	0.05	0.10	0.20	0.30	0.40	Zmax	θ max
D8S550	- infini	-1.23	0.76	1.08	0.79	0.38	0.12	1.0956	0.104
D8S1759	3.06	2.94	2.48	1.95	1.10	0.52	0.16	3.0611	0.001
D8S265	2.61	2.53	2.17	1.74	0.99	0.44	0.12	2.6611	0.001
D8S552	4.86	4.70	4.06	3.28	1.88	0.83	0.23	4.8435	0.001
D8S1790	2.88	2.77	2.34	1.84	1.04	0.48	0.14	2.8800	0.000
D8S1754	-1.54	-0.12	0.87	1.06	0.84	0.46	0.15	1.0694	0.106
D8S511	4.21	4.66	4.54	3.91	2.46	1.20	0.37	4.7253	0.021
D8S1827	2.40	2.88	2.87	2.45	1.53	0.76	0.24	2.9764	0.025
D8S549	1.94	2.53	2.83	2.58	1.73	0.90	0.30	2.8352	0.044
D8S1731	6.35	4.73	6.38	5.51	3.64	1.97	0.73	6.7476	0.015
D8S261	6.12	6.82	6.57	5.73	3.81	2.02	0.68	6.8673	0.018
D8S1715	1.16	1.11	0.92	0.71	0.39	0.17	0.05	1.1518	0.001
D8S280	-infini	-3.20	-0.90	-0.18	0.13	0.09	0.02	0.1306	0.215
D8S282	-infini	-4.61	-1.16	-0.11	0.33	0.24	0.08	0.3321	0.209

B.

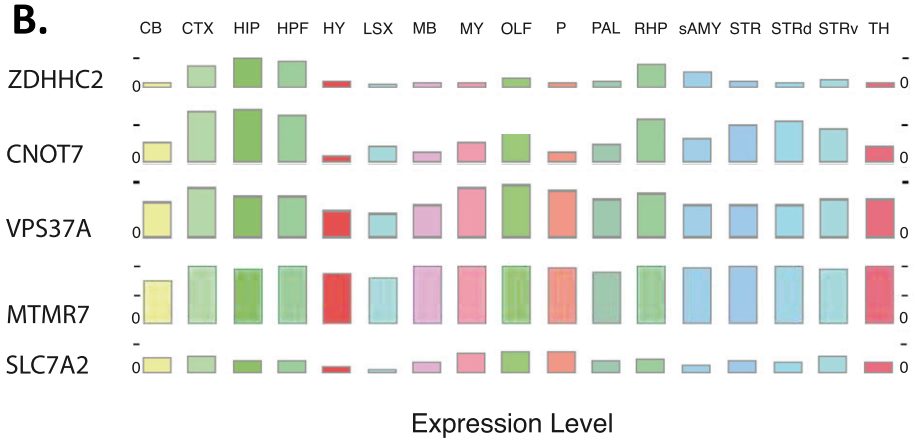

Fig. S2. Locus identification and candidate gene hunting. (*A*) Pairwise-LOD scores were calculated using the MLINK program (1). Flanking markers D8S550 and D8S280 are 20.31 cM apart (9.5 Mb). Haplotype reconstruction and additional markers were used to reduce the candidate interval to the minimal overlapping region of homozygosity, flanked by D8S1731 and D8S261 microsatellites. (*B*) Pattern of brain expression of candidate genes. Scaled expression level ranging 0; 50% and 100% of in situ hybridization are plotted for each studied gene from the locus: *ZDDHC2*, *CNOT7*, *VPS37A*, *MTMR7* and *SLC7A2*, in a sagittal plane of brain in a male C57BL/6 mouse aged 55 d (Allen Human Brain Atlas, http://www.brain-map.org). Each expression level is calculated on centered structures indicated at the top of the graph and comprising cerebellum (CB), cortex (CTX), hippocampus (HIP), hippocampal formation structure (HPP), hypothalamus (HY), lateral septal compex structure (LSX), midbrain (MB), olfactory bulb structure (OLF), pons (P), pallidum structure (PAL), retrohippocampal region structure (RHP), striatum like amygdala nuclei structure (sAMY), striatum structure (STR), striatum dorsal region structure (STRd), striatum ventral region structure (STRv), and thalamus structure (TH).

1. Lathrop GM, Lalouel JM, Julier C, Ott J (1985) Multilocus linkage analysis in humans: Detection of linkage and estimation of recombination. *Am J Hum Genet* 37:482–498.

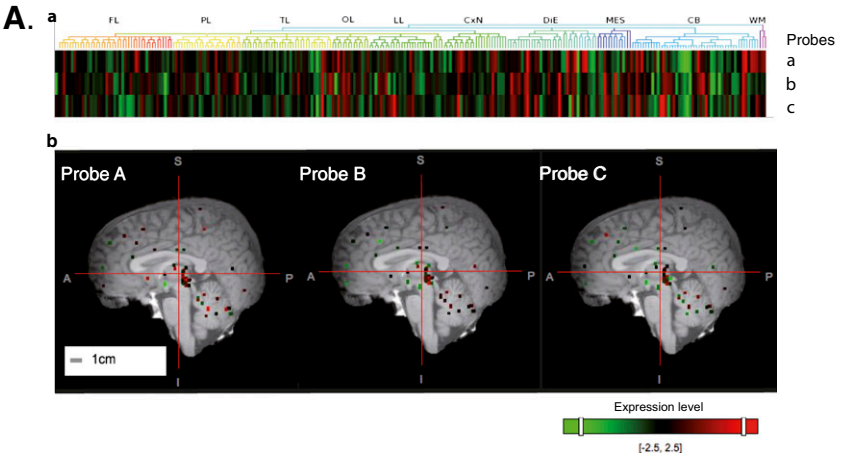

B. exonization ?

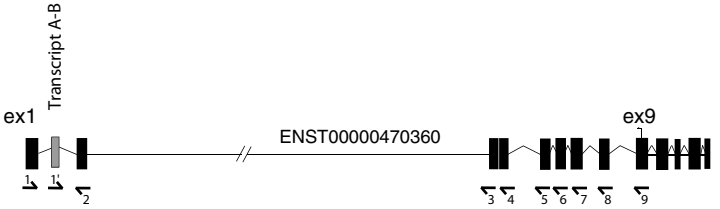

primers	expected size (bp)	observed size (bp)
ex1ex2		
F TCCTCTTCCCGGGACCAGC	154	154 (WT,M)
F' ATTGACAAAACGCAGCCAAAT	216	no band (WT,M)
R TGCTTTCCTGCTGGTCTTC		
ex1ex3		
F TCCTCTTCCCGGGACCAGC	204	204 (WT,M)
F' ATTGACAAAACGCAGCCAAAT	266	no band (WT,M)
R TTTCGTGGTGAGACATCTGCT		
ex1ex4		
F TCCTCTTCCCGGGACCAGC	443	443 (WT,M)
F' ATTGACAAAACGCAGCCAAAT	505	no band (WT,M)
R GTGGATAAGCAGCGGCATAAT		
ex1ex5		
F TCCTCTTCCCGGGACCAGC	823	823 (WT,M)
F' ATTGACAAAACGCAGCCAAAT	885	no band (WT,M)
R CTGCAAGACCAGTGTAATTCAT		
ex1ex6		
F TCCTCTTCCCGGGACCAGC	973	973 (WT,M)
F' ATTGACAAAACGCAGCCAAAT	1035	no band (WT,M)
R CTTTCACAAACCCAGCAACCA		
ex1ex7		
F TCCTCTTCCCGGGACCAGC	1103	1103 (WT,M)
F' ATTGACAAAACGCAGCCAAAT	1165	no band (WT,M)
R CCCGTAAAGCCATAAGGCATA		
ex1ex8		
F TCCTCTTCCCGGGACCAGC	1336	1336 (WT,M)
F' ATTGACAAAACGCAGCCAAAT	1398	no band (WT,M)
R ATCCCACATATTCAAACGCTAC		
ex1ex9 SLC7A2 variant 1		
F TCCTCTTCCCGGGACCAGC	1531	1531 (WT,M)
F' ATTGACAAAACGCAGCCAAAT	1593	no band (WT,M)
R CACTGCACCCGATGATAAAGT		

C.

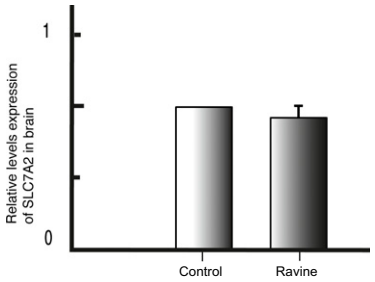

Fig. S3. Expression of SLC7A2 in brain. (*A*). Pattern of expression of *SLC7A2* in different brain samples. (*a*) Whole-brain microarray experiments from a same donor (male, aged 24 y, African American, PMI:23 h) using three distinct probes. Data presented under heat-map format are normalized data across the entire set of microarray samples. Red to green color is indicative of *z*-score from respectively frontal lobe (FL), parietal lobe (PL), temporal lobe (TL), occipital lobe (OL), limbic lobe (LL), cerebral cortex (CC), diencephalon (DiE), midbrain (Mes), cerebellum (CB), white matter (WM). (*b*) Three-dimensional planar view of *SLC7A2*. Expression was reproducible with all probes in cerebellum and midbrain. Spatial correspondences between images and T1 weighted MR volumes were obtained via a series of assisted registration processes. Images and methods are accessible in the Allen Human Brain Atlas. A, B, and C probes are all located in *SLC7A2* on chromosome 8 and respectively span from 17,412,117–17,412,176, 17,419,598–17,421,149, and 17,415,803–17,415,856 (hg19). (*B*) *SLC7A2* alternative isoforms. PCR amplification was performed using standard conditions. The same forward primer was used in exon 1 in association with different reverse

Legend continued on following page

primers in exons 2, 3, 4, 5, 6, 7, 8, and 9 of *SLC7A2*. No difference was observed between the expected and observed sizes of PCR products in either patient (M) or control (WT) cDNA. Sequencing analysis was used to confirm the absence of variation. (*C*) *SLC7A2* expression was assessed by qRT-PCR in brain samples and revealed no significant difference between Ravine brain tissue (patient) and control.

Fig. S4. Cloning of unique noncoding RNA in human brain. FASTA-formatted sequences of A and B isoforms. 3′- and 5′-RACE were carried out using total RNA isolated from human brain that led to the cloning of two unique transcripts A and B, which were 1,536-nt and 962-nt long, respectively. siRNA sequences used in knockdown experiments are underlined with their names below. Squared A indicates the position of the A > G mutation. Italicized letters and bold letters indicate the AluSz and the L1PA8 elements, respectively.

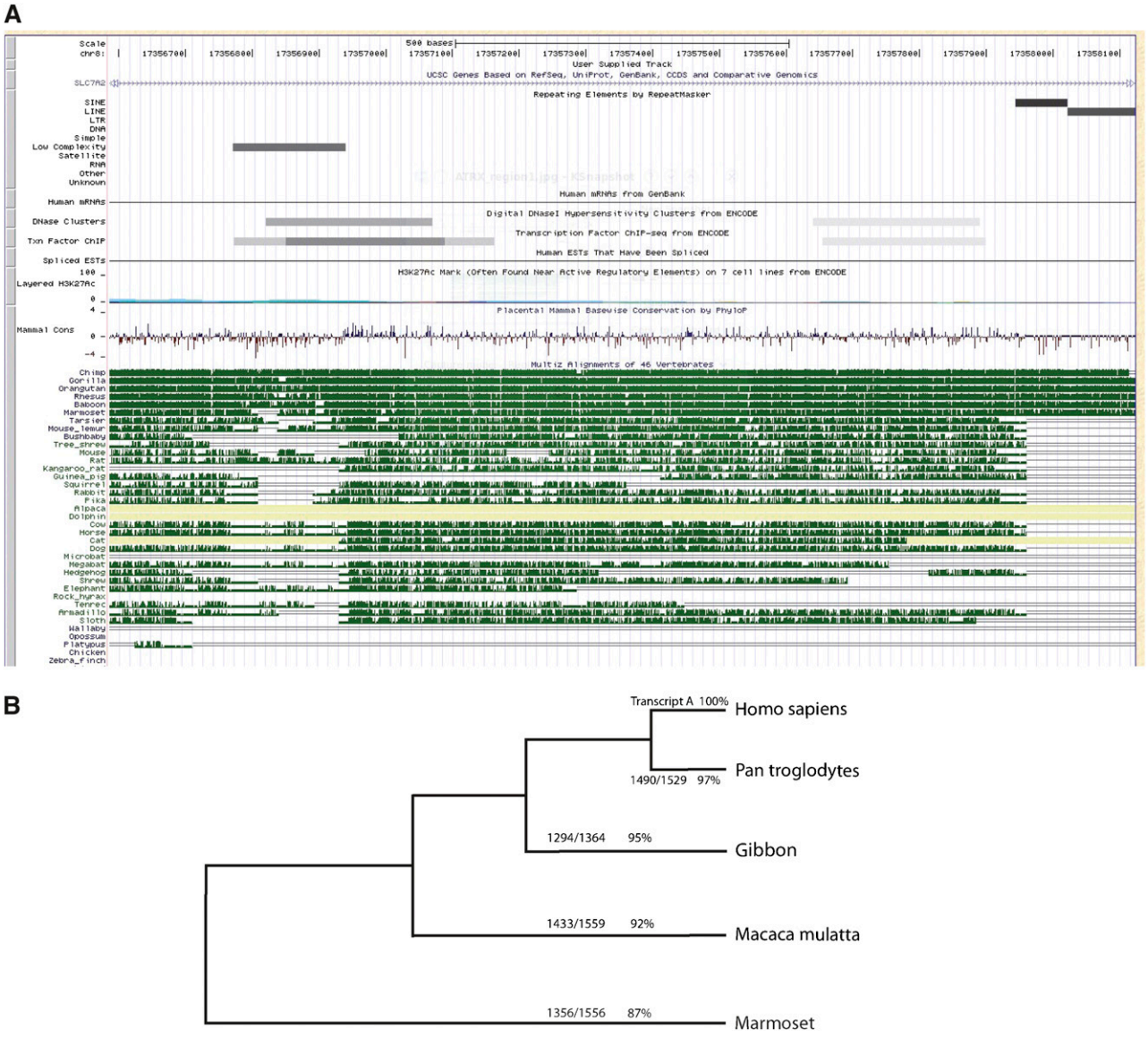

Fig. S5. Conservation of SLC7A2-IT1A/B in primates. (*A*) Homology-spanning of the full-length transcript A sequence can be observed among all primates but not in other species. Shown are direct results from the University of California at Santa Cruz (UCSC) browser (http://genome.ucsc.edu/) using UCSC hg19 46-species MultiZ track. (*B*) BLAST results of *SLC7A2-IT1A* sequence against primate genomes are indicated on a phylogenetic tree in primates. Identities that were calculated using Megablast from National Center for Biotechnology Information (http://www.ncbi.nlm.nih.gov/blast/) are indicated as a ratio. *SLC7A2-IT1A* was compared with primate genome builds from marmoset (*Callithrix jacchus*, build 1.1), chimpanzee (*Pan troglodytes*, build 3.1), macaque (*Macaca mulatta*, build 1.2), and gibbon (*Nomascus leucogenys*, build 1.1).

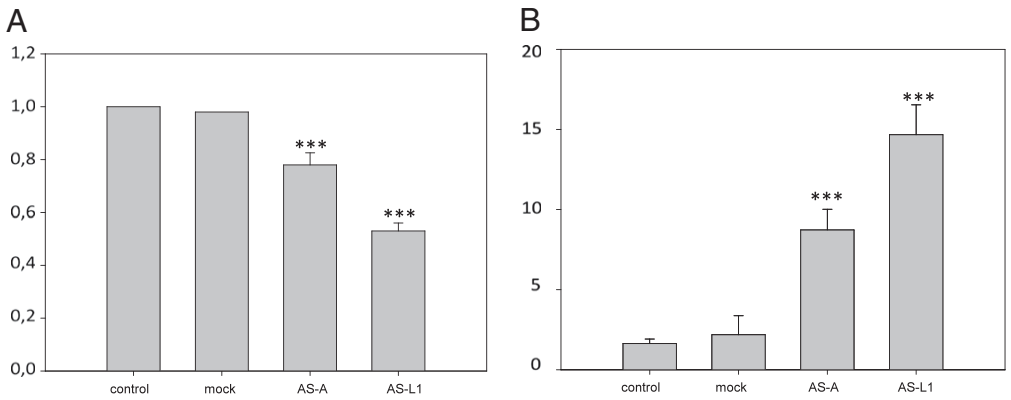

Fig. S6. Knockdown of SLC7A2-IT1A/B transcripts and effect on apoptotic markers. Human neuroblastoma Kelly cells were transfected with antisense phosphorothioate oligonucleotide specific to the A sequence (AS-A) or to the L1 subregion (AS-L1) at different concentrations (25, 50, and 100 nM) during a time course of 12, 24, and 48 h. Strongest antisense effect was obtained at 24 h for the 50-nM concentration of each antisense oligonucleotide. (*A*) Kelly cells were not transfected (control) or transfected with either scrambled oligonucleotide (mock), AS-A, or AS-L1. Real-time PCR analysis was performed to assess relative *SLC7A2-IT1A/B* levels. *GAPDH* served as the control for normalization. Antisense oligonucleotides resulted in a decrease of *SLC7A2-IT1A/B* RNA by 22% and 47% using AS-A and AS-L1, respectively. (*B*) Apoptotic response was determined by counting the percentage of cells double stained for mitochondrial Bax and cleaved Caspase 3. All results are expressed as mean of percentage ± SD of three independent microscope field counts, each in triplicate. Apoptotic response reached 8.7% and 14.6% with AS-A and AS-L1, respectively, which were both significantly increased compared with mock (***$P < 0.01$, $n = 3$).

Table S1. Summary of clinical features of patients

Patients	Sex	Affected siblings	Age at onset anorexia with emesis (mo)	Weight at 1 y old < −2 SD	Pyramidal syndrome	Ataxia spasticity	Abnormal ocular motility	Laryngeal paralysis	Apnea	BAEP abnormalities	Age at first seizures (y)	Age at death (y)	MRI abnormalities
7	F	+	6	+	+	—	—	+	+	NA	NA	2	NA
728	F	+	9	+	+	+	—	NA	NA	+	NA	—	+
537	M	+	5	+	+	+	+	—	+	+	—	2	+
668	M	+	5	+	+	+	—	—	—	+	6	—	+
624	M	+	9	+	+	+	+	NA	NA	NA	—	—	+
953	M	—	6	+	+	+	+	—	—	+	5	16	+
571	F	+	6	+	+	+	+	—	—	NA	—	—	+
572	F	+	8	+	+	+	+	—	—	—	—	22	NA
615	M	+	5	+	+	—	—	—	NA	—	—	—	+
613	M	+	11	+	+	+	+	—	NA	NA	15	—	+
682	M	—	7	+	+	—	+	—	—	+	—	—	+
505	F	—	6	+	+	+	—	—	—	+	—	—	+
776	F	—	9	+	+	+	+	—	NA	NA	—	23	NA
691	F	—	8	+	+	+	+	—	—	+	—	—	+
518	M	—	6	+	—	+	+	+	NA	—	—	2	NA

+, present; —, absent; BAEP, brainstem auditory evoked potentials; CSF, cerebrospinal fluid; NA, not available.

Table S2. Summary of computational analyses

Analyses	Tools	References	Scan of mutant vs. wild-type *SLC7A2-IT1A/B* sequence
Exon scan*	ExonScan Web Server	(1)	No change
Intron/exon structure*	Genscan	(2)	No change
Alternative splicing*	ProSplicer	(3)	No change
Splice information*	RegRNA	(4)	No change
Transcription factors binding sites*	MatInspector	(5)	No change
MicroRNA targeting*	RegRNA	(4)	No change
MicroRNA targeting*	microInspector	(6)	No change
Transcriptional regulatory elements*	GPMiner	(7)	No change
Functional elements in noncoding sequence*	Systematic approach	(8)	No change
MicroRNA precursor-seeking programs†	Mireval	(9)	WT, –; Mut, +
	miPred	(10)	WT, –; Mut, +
	mirAlign	(11)	WT, –; Mut, +
	miRNAminer	(12)	WT, –; Mut, +
	microPred	(10)	WT, –; Mut, +
	RNAmicro	(13)	WT, –; Mut, +

*Scanning procedure integrated the listed computational methods to comprehensively annotate putative transcription start site, first exon end position, transcription factor binding site, CpG island, G + C content, TATA box, CCAAT box, GC box, statistical overrepresented oligonucleotide, DNA stability, intronic and exonic enhancer and silencer, and microRNA target sites.

†Computing *SLC7A2-IT1*A/B sequences revealed that the mutant (Mut) but not the wild-type sequence (WT) comprised a pseudo-microRNA precursor encompassing the mutation, as assessed by seven distinct computing methods comprising the RNA self-containment (Fig. S6).

1. Wang Z, et al. (2004) Systematic identification and analysis of exonic splicing silencers. *Cell* 119:831–845.
2. Burge CB (1998) Modeling dependencies in pre-mRNA splicing signals. *Computational Methods in Molecular Biology*, eds Salzberg S, Searls D, Kasif S (Elsevier Science, Amsterdam), pp 127–163.
3. Huang HD, Horng JT, Lee CC, Liu BJ (2003) ProSplicer: A database of putative alternative splicing information derived from protein, mRNA and expressed sequence tag sequence data. *Genome Biol* 4:R29.
4. Huang HY, Chien CH, Jen KH, Huang HD (2006) RegRNA: An integrated web server for identifying regulatory RNA motifs and elements. *Nucleic Acids Res* 34(Web Server issue): W429–W434.
5. Cartharius K, et al. (2005) MatInspector and beyond: Promoter analysis based on transcription factor binding sites. *Bioinformatics* 21:2933–2942.
6. Rusinov V, Baev V, Minkov IN, Tabler M (2005) MicroInspector: A web tool for detection of miRNA binding sites in an RNA sequence. *Nucleic Acids Res* 33(Web Server issue): W696–W700.
7. Lee TZ, Chang WC, Hsu JBK, Chang TH, Chien DM (2012) GPMiner: An integrated system for mining combinatorial cis-regulatory elements in mammalian gene group. *BMC Genomics* 13(Suppl 1):S3.
8. Lomelin D, Jorgenson E, Risch N (2010) Human genetic variation recognizes functional elements in noncoding sequence. *Genome Res* 20:311–319.
9. Ritchie W, Théodule FX, Gautheret D (2008) Mireval: A web tool for simple microRNA prediction in genome sequences. *Bioinformatics* 24:1394–1396.
10. Han K (2011) Effective sample selection for classification of pre-miRNAs. *Genet Mol Res* 10:506–518.
11. Wang X, et al. (2005) MicroRNA identification based on sequence and structure alignment. *Bioinformatics* 21:3610–3614.
12. Artzi S, Kiezun A, Shomron N (2008) miRNAminer: A tool for homologous microRNA gene search. *BMC Bioinformatics* 9:39.
13. Hertel J, Stadler PF (2006) Hairpins in a Haystack: Recognizing microRNA precursors in comparative genomics data. *Bioinformatics* 22:e197–e202.

Dataset S1. Compilation of short genetic variations comprised in the Ravine locus and their genotypes

Dataset S1 (xls)